

# Thermodynamic Studies of Two-Dimensional Correlated Electron Systems

V. M. Pudalov<sup>1,2</sup> · A. Yu. Kuntsevich<sup>1,2</sup> ·  
I. S. Burmistrov<sup>2,3</sup> · M. Reznikov<sup>4</sup>

Received: 15 July 2015 / Accepted: 29 July 2015 / Published online: 19 August 2015  
© Springer Science+Business Media New York 2015

**Abstract** This paper describes recent developments in experimental techniques for thermodynamic measurements. Particularly, we focus on the derivatives of the chemical potential with respect to magnetic field and temperature. The former enables to determine the spin magnetization per electron and the latter the entropy per electron. We briefly describe recent results obtained with these techniques and their impact on the current understanding of the still challenging problem of the ground state(s) of strongly correlated two-dimensional electron systems.

**Keywords** Two-dimensional electron system · Strongly correlated electron systems · Thermodynamic measurements

## 1 Introduction

Low temperature thermodynamic properties (TD) of materials carry rich information about inter-particle correlations. In contrast to ubiquitous transport and optical studies, interpretation of thermodynamic data is straightforward and is often model independent. However, due to the additive character of thermodynamic properties, their measurements require substantial amount of material, or, alternatively, extremely high sensitivity of the measurement technique. This becomes the main

---

✉ V. M. Pudalov  
pudalov@sci.lebedev.ru

<sup>1</sup> P.N. Lebedev Physical Institute of the RAS, 119991 Moscow, Russia

<sup>2</sup> Moscow Institute of Physics and Technology, 141700 Moscow, Russia

<sup>3</sup> L.D. Landau Institute for Theoretical Physics, 119334 Moscow, Russia

<sup>4</sup> Solid State Institute, Technion, 32000 Haifa, Israel

obstacle for studying thin films, two-dimensional (2D) electron sheets, and other nanometer-size systems where the number of particles does not exceed  $10^8$ – $10^{10}$ . Another problem accompanying traditional thermodynamic measurements is the necessity to eliminate the contribution of a substrate to the measured TD properties, which becomes of crucial importance in the case of thin films or small-sized systems.

About three decades ago a method has been developed for measuring TD properties of two-dimensional electron layers [1–4]. The method aimed primarily at chemical potential measurements is based on the Thomson (Lord Kelvin) idea [5] that when two plates of a capacitor are made of materials with different chemical potentials  $\mu_{1,2}$ , the charge of the plates is  $C(\mu_1 - \mu_2)/e$ , where  $C$  is the electric capacitance. Correspondingly, when the two plates are connected electrically and an external parameter varies affecting one of the chemical potential values, a recharging current flows between the plates.

For definiteness we shall consider 2D electron layers [6]. A cross section of the typical Si-MOSFET sample is shown schematically in Fig. 1. The upper plate of the plane capacitor (“gate”) is an Al-film deposited on the  $\text{SiO}_2$  layer. As a positive gate voltage is applied to the gate, electrons fill in the narrow potential well at the Si– $\text{SiO}_2$  interface. Their motion therefore is free only in the  $X$ – $Y$  plane, and restricted (quantized) in the  $Z$ -direction. For a low enough electron density only the lowest size quantization subband is filled, and electrons form a two-dimensional sheet with a thickness of the Fermi wavelength. A great advantage of this gated structure is a possibility to tune the electron density in a wide range,  $10^{10}$ – $10^{13}$   $\text{cm}^{-2}$ , simply by varying the voltage applied to the gate [6].

The recharging current  $j$  of such a capacitor is always proportional to  $\Delta\mu$ , whose variations are related to the chemical potential of the 2D electron gas solely. When  $\mu$  changes due to electron gas density variations  $\delta n$  [4, 7], the current  $j$  is proportional to  $(\partial\mu/\partial n)$ ; for magnetic field variations  $\delta B$ ,  $j \propto (\partial\mu/\partial B)$  [1, 8, 9], and for temperature variations  $\delta T$ ,  $j \propto (\partial\mu/\partial T)$  [10–12], etc. Thereby, in the first case one can measure the electron compressibility (or, by integrating it—density dependence of  $\mu$ ), in the second case the electron magnetization per electron (or field dependence of  $\mu$ ), and in the third case the entropy per electron (or temperature dependence of  $\mu$ ). For short, by “magnetization per electron” and “entropy per electron,” we mean  $dM/dn$  and  $dS/dn$ , respectively.

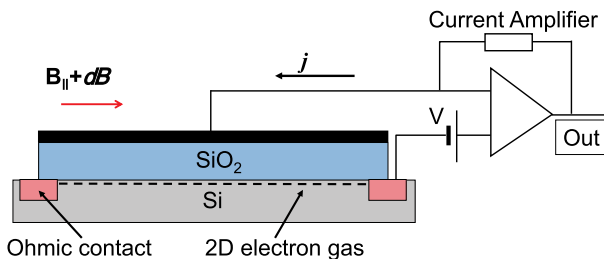


**Fig. 1** Schematic cross section of the Si-MOSFET sample, and experimental set-up of the spin magnetization measurements [9, 30] (Color figure online)

## 2 Ground State Energy

Correlations play a crucial role for electrons moving in a neutralizing charge background [13]. Their importance grows both with lowering the density and the space dimensionality and renders the simple schemes, such as the Hartree–Fock (HF) or the random-phase approximation (RPA) [13], inapplicable. In the low-density strongly correlated electron liquid, the energy balance determining the system properties is played on a very minute scale and, to get meaningful predictions, a great accuracy such as the one afforded by quantum Monte Carlo (QMC) methods is necessary [13].

The ground-state properties of 2D electron systems (2DES) have been studied under various approximations such as RPA and summation of ladder diagrams by several authors. In particular, the variational and fixed-node Green's-function Monte Carlo calculations have been performed [14] for the two-dimensional clean electron gas in the interaction range  $1 < r_s < 100$  (both interaction strength and density are commonly characterized with a dimensionless parameter  $r_s$ , that is equal to the ratio of Coulomb interaction energy to the kinetic energy for a single-valley 2D system,  $r_s \propto 1/\sqrt{n}$  [6]). The calculations [14] predicted a Wigner crystallization at  $r_s = 37 \pm 5$ . The electron system is found to be in the normal-(paramagnetic) fluid state below the transition density, but with the fully polarized state being very close in energy. The accuracy of the numerical calculations, however, is far insufficient to predict reliably the spin-polarization transition, and this issue remains challenging.

Disorder effect on the ground state is even a more subtle issue. Obviously, the residual disorder, whatever weak, is expected to pin the Wigner crystal (WC) rendering the system an insulator. It is known also that weak disorder stabilizes the Wigner crystal due to creation of a gap in the phonon spectrum and hence limiting zero-point displacements [15].

Eguiluz, Maradudin, and Elliott considered a two-dimensional Wigner lattice in the presence of a random array of pinning centers and of a static external magnetic field perpendicular to the lattice [15]. They presented detailed numerical results for the phonon spectral density and electron mean-square displacement, both at  $T = 0$  and at finite temperatures.

Chui and Tanatar [16, 17] investigated the effect of impurities on the electron liquid–solid transition via perturbation calculations and Monte Carlo simulations. Disorder (impurities concentration and their set-back distance) was chosen to correspond to high mobility Si-MOSFETs studied in [18]. The critical density for Wigner crystallization  $r_s$  was found to shift from 37 to 7.5 for which there is about 100 electrons per impurity, and this case is far from the situation when each electron resides on its impurity (the latter is considered as the strongly localized state). It is not surprising, therefore, that the short-range spatial order is well pronounced in the system. However, as the electron density is reduced, finally, the short-range order is gradually lost and the 2D system approaches the above-mentioned strongly localized state. In the simulations, the critical  $r_s \approx 7.5$  value is close to the observed experimental results [18]. Near the solid–liquid transition  $r_s = 7.5$  the system is crystalline and rapidly becomes quite amorphous as  $r_s$  is further decreased.

By now there is no experimental technique to measure the ground state energy. Only the energy derivatives with respect to various parameters are experimentally accessible;

they are considered below. We hope that bringing together the pieces of information available from various thermodynamic measurements will help in composing a comprehensive realistic picture of the interacting and disordered low-dimensional electron systems.

### 3 Compressibility

The inverse compressibility (or  $\partial\mu/\partial n$ ) of a system reflects the chemical potential variations with density:

$$\kappa^{-1} = n^2 \frac{\partial^2 E_{\text{tot}}}{\partial n^2} = n^2 \left( \frac{\partial\mu}{\partial n} \right).$$

For non-interacting electrons  $\kappa$  is proportional to the single-particle density of states (DOS), which in 2D is density independent, being  $(g_v m / (\pi \hbar^2))$  ( $g_v$ —is the valley degeneracy) [6]:

$$\kappa^{-1} = n^2 \frac{\pi \hbar^2}{g_v m} \quad (1)$$

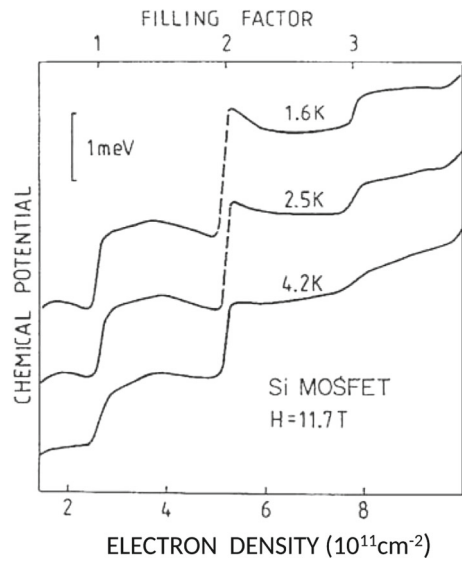
This picture, however, changes drastically when interactions are included. It was realized already in the 1980s that compressibility of a 2DES can become negative at low densities, owing to the electron-electron interactions [19]. Exchange and correlation effects weaken the repulsion between the electrons, thereby reducing the energy cost, thus leading to negative and singular corrections to  $\partial\mu/\partial n$ . At zero magnetic field this effect is primarily due to the exchange energy, while in high fields the correlation energy plays a significant role as well [20]. Within the HF theory

$$\frac{\partial\mu}{\partial n} = \frac{\pi \hbar^2}{m} - \left( \frac{2}{\pi} \right)^{1/2} \frac{e^2}{4\pi\epsilon} \frac{1}{n^{1/2}}. \quad (2)$$

Thus, upon decreasing density, the compressibility gets negative. Experimentally, this behavior has been found first in the capacitance and chemical potential measurements in magnetic field [8, 21, 22]. Later it was confirmed in the zero field compressibility measurements performed by a more elaborated field penetration technique (requiring double-gated samples) [23–26]. All these data demonstrate that the compressibility of an interacting two-dimensional electron system becomes indeed negative as the interaction strength exceeds  $r_s \approx 1 - 2$ . Physically, the state with negative compressibility means that when electrons are added to the system, the gain due to the exchange and correlation prevails and exceeds the loss due to increasing kinetic (Fermi) energy, and as a result the total energy decreases.

The negative compressibility is enhanced in the presence of a quantizing perpendicular magnetic field [22], where it reaches maxima at shoulders of the Landau levels. Figure 2 shows that the chemical potential exhibits jumps as the electron density passes through complete filling of the Landau levels (QHE conditions). Importantly, at low

**Fig. 2** Chemical potential of Si-MOSFET sample at three temperatures. *Upper horizontal axis*—Landau level filling factors, *lower axis*—approximate electron density [22]. The curves are shifted vertically, for clarity (Color figure online)



temperatures there is a downturn of  $d\mu/dn$  at filling factors right below and above the jumps, so their amplitude is significantly enhanced, in accordance with the theoretical prediction [27]. This is the result of the negative compressibility, which is most pronounced on the shoulders of the filled Landau levels. Thus, the negative  $\partial\mu/\partial n$  manifests here as a negative slope of the  $\mu(n)$  curves.

#### 4 Spin Magnetization

An interacting low-density electron system has a tendency to magnetic ordering which is determined by the interplay between the electronic Coulomb interaction and Pauli principle. As density decreases, the ratio  $r_s$  between the interaction and Fermi energies increases pushing the system towards a ferromagnetic instability.

In the Hartree-Fock approximation the Bloch instability, a first-order phase transition from unpolarized to fully polarized state, happens at unrealistically small  $r_s \approx 2$ . In the opposite limit of short-range interactions, the Stoner instability, a second-order phase transition characterized by divergent spin susceptibility, is expected. The hierarchy of these transitions is discussed in [28] within the RPA approximation. Numerical simulations for a clean single-valley two-dimensional electron system (2DES) [29] predict a Bloch instability at  $r_s \approx 25$  followed by Wigner crystallization at  $r_s \approx 37$ , whereas a clean two-valley system is believed to be stable against spontaneous spin polarization. Spin magnetization measurements [30–32], especially those performed in weak magnetic field [9], have addressed this issue experimentally.

We note that there is a large body of experimental studies of the spin magnetization in perpendicular magnetic fields, where the magnetization is large due to orbital effects, and spin magnetization is greatly enhanced due to interactions. These effects were extensively studied in the context of the Quantum Hall Effect physics. In this section,

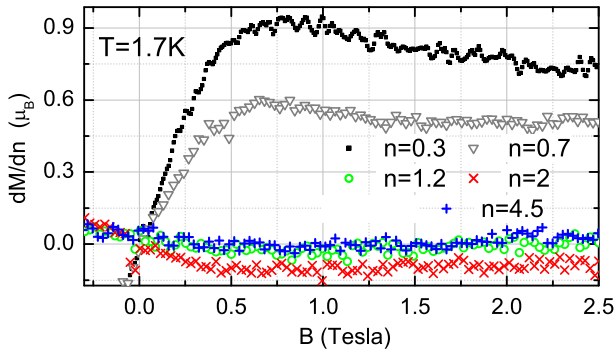


**Fig. 3**  $\partial M/\partial n$  versus  $B$  at different densities and at  $T = 1.7\text{K}$ . Density is units of  $10^{11}\text{ cm}^{-2}$  (Color figure online)

rather, we focus on the low-field and zero field spin magnetization and do not consider measurements in perpendicular magnetic field.

When a magnetic field is applied in the 2D plane, it couples to the electron spins solely. In this geometry spin magnetization has been measured in several experiments [9, 30–32]. A typical experimental set-up is shown in Fig. 1. Here magnetic field  $\mathbf{B}$  is applied in the 2D plane. A small modulation field  $\delta\mathbf{B} \approx 40\text{ mT}$  causes recharging current to flow  $\delta j = -\delta\mathbf{B}(i\omega C/e)(\partial\mu/\partial B)$ . Here  $C$  is the total sample capacitance and  $\omega/2\pi = (4\text{--}12)\text{ Hz}$  is the modulation frequency. Due to the Maxwell relation  $(\partial M/\partial n) = -(\partial\mu/\partial B)$ , the spin magnetization per electron is obtained from the measured recharging current  $j$  [9, 30–32]. The thermodynamic measurements are possible not only at high electron density in the well-conducting regime but also deep in the localized phase; in the latter case the capacitance  $C$ , that enters the recharging current equation, should be taken complex, as appears in measurements [32].

The main result of these measurements is the observation of “spin-droplets”—spin polarized collective electron states with a total spin of the order of 2 [9]. These easily polarized “nanomagnets” exist as a minority phase on the background of the majority Fermi liquid phase even though the density and the dimensionless conductance  $k_{Fl} \sim 100 \gg 1$  are high; the latter inequality is commonly considered as a criterion of a well-defined Fermi liquid state.

Figure 3 shows typical  $\partial M/\partial n$  signal for several densities. To get insight into the observed behavior of  $\partial M/\partial n$  as a function of the density, we review two limiting cases (i) of low and (ii) of very high densities.

- (i) For low densities  $\partial M/\partial n$  is positive, much exceeding the Pauli spin susceptibility. Its magnetic field behavior is reminiscent of that anticipated for free spins,  $\partial M/\partial n = \mu_B \tanh(b)$ , where  $b = \mu_B B/k_B T \ll 1$  is the dimensionless magnetic field. However, as temperature decreases,  $\partial M/\partial n$  exceeds Bohr magneton, the fact that evidences for ferromagnetic alignment of spins. Moreover, the magnetization curves,  $\partial M/\partial n$  versus  $b$ , “saturate” in fields  $b \approx 0.25$  rather than unity, signifying a large total spin,  $S \sim 1/2b = 2$ , of the collective easily magnetized states responding to the field modulation.

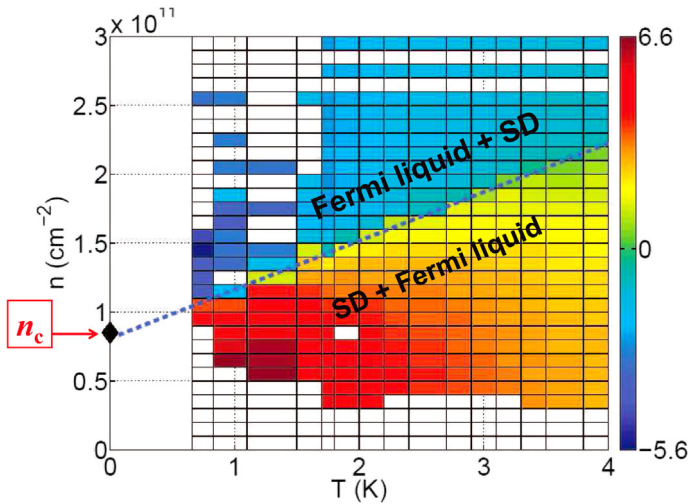


**Fig. 4** Phase diagram of the spin susceptibility  $\partial\chi/\partial n$  represented in colors for each temperature and density, in units of  $(\mu_B/T)$ . Dashed blue line represents the density at which  $\partial\chi/\partial n$  is zero. Black diamond depicts the critical density of the metal-insulator transition,  $n_c$ , known from transport measurement [9]. (Color figure online)

- (ii) For high densities, deep in the metallic regime, the ratio between interaction and the Fermi energies is small. One expects to get the density-independent Pauli spin susceptibility in low magnetic field, and as a result  $\partial M/\partial n$  approaches zero, as may be seen in Fig. 3 for  $n = 2$  and  $4.5 \times 10^{11} \text{ cm}^{-2}$ .

At the intermediate densities, well inside the metallic phase, e.g., at  $n = 1.5 \times 10^{11} \text{ cm}^{-2}$ , the low temperature  $\partial M/\partial n$  changes sign. Note that negative  $\partial M/\partial n$  is expected in the metallic phase, since increase in density reduces interaction and therefore spin polarization of a 2D electron system. Thermal fluctuations also suppress magnetic ordering; therefore,  $\partial M/\partial n$  becomes less negative with temperature and, at temperatures exceeding the Fermi energy (about 10K at  $n = 1.5 \times 10^{11} \text{ cm}^{-2}$ ), approaches the dependence expected for non-interacting electrons.

Figure 4 shows a color-phase diagram, where the critical dashed line corresponding to the sign change of the spin-susceptibility-per electron,  $\partial\chi/\partial n$ , separates the regions with dominating spin droplets and Fermi liquid states, respectively. In the lower-density phase, as the density increases the number of droplets also increases, reaching its maxima at the temperature-dependent critical density shown by the dash line in Fig. 4. In the high-density phase the spin droplets melt with the density. The phase diagram, therefore, signifies a critical magnetic behavior. Interestingly, the dashed critical line in the  $T = 0$  limit extrapolates to the critical density value  $n_c$  for the metal-insulator transition in transport. The coincidence of the magnetic and transport critical density values at  $T \rightarrow 0$  suggests that the two phenomena, the formation of easily magnetized droplets and the metal-insulator transition in transport, are intimately interrelated; the origin of this link is not clarified yet.

No signatures of the presence of ferromagnetic droplets are detected so far in transport in the metallic phase, e.g., dephasing time shortening. We believe this is due to the

fundamental difference between the physical quantities provided by thermodynamic and transport methods: the thermodynamic method yields an average magnetization of all the electrons that are capable of recharging within about hundred millisecond field modulation period. In contrast, the transport is influenced mostly by delocalized electrons having the picosecond-scale relaxation time.

## 5 Entropy Measurements

For  $\partial\mu/\partial T$  measurements we apply the technique similar to that described above for the 2D electron systems in magnetic field and also to the one used for the bulk samples in Ref. [10]. Instead of magnetic field modulation, as in Fig. 1, we modulated the sample temperature. The heater varies the temperature  $T$  of a sample (either Si-MOSFET or GaAs-FET), as  $T(t) = T_0 + \Delta T \cos(\omega t)$ . Both  $T_0$  and  $\Delta T$  values were measured using a miniature thermometer attached to the copper sample chamber; the sample capacitance  $C$  was determined in the same experiment. Temperature  $T_0$  varied from 2.4 to 26 K and was modulated at the frequency  $\omega/(2\pi) \approx 0.5$  Hz with the amplitude  $\Delta T \approx 0.1 - 0.2$  K. Modulation of the sample temperature changes the chemical potential and, hence, causes recharging of the gated structure. Therefore,  $\partial\mu/\partial T$  is directly determined in the experiment from the measured recharging current:  $j(t) = (\partial\mu/\partial T)\Delta T\omega C \sin(\omega t)$ . Using the Maxwell relation,

$$(\partial S/\partial n)_T = -(\partial\mu/\partial T)_n,$$

the density derivative of the entropy is found from the temperature derivative of the chemical potential.

We first focus on  $\partial\mu/\partial T$  oscillations in weak perpendicular fields to compare them with the semiclassical theory and to determine the shape of the level's density of states.

It is worthwhile to give a qualitative explanation why  $\partial\mu/\partial T$  oscillates with perpendicular magnetic field when the gate voltage is kept constant. For the bare quadratic energy spectrum,  $\varepsilon(p) = p^2/2m$ , the single electron density of states is constant in two dimensions. At temperatures  $T \ll E_F$  the number of particle-like excitations above  $\mu$  equals to the number of hole-like excitations below  $\mu$  (hatched areas in Fig. 5a). Therefore, for a fixed electron density  $n$  the chemical potential is independent of temperature,  $\partial\mu/\partial T = 0$ , with exponential accuracy at low temperatures,  $T \ll E_F$ .

In the case of energy-dependent density of states (e.g., in 3D systems, graphene or 2D systems with non-parabolic spectrum, or in quantizing magnetic field), one can expand it in the vicinity of the Fermi energy (see Fig. 5b):  $D(\varepsilon) = D(E_F) + (\partial D(\varepsilon = E_F)/\partial\varepsilon) \times (\varepsilon - E_F)$ . Then, for a non-zero temperature the hatched areas in Fig. 5b are not equal, the particle-hole asymmetry emerges, and the chemical potential shifts in order to conserve the total number of particles. Using the standard low temperature expansion for the Fermi type integrals (see, e.g., Ref. [33]), one can easily find correction to the chemical potential at low temperatures,  $T \ll E_F$ :

$$\mu(T) - E_F = -[\pi^2 T^2 / 6D(E_F)] \times \partial D(\varepsilon = E_F) / \partial\varepsilon.$$

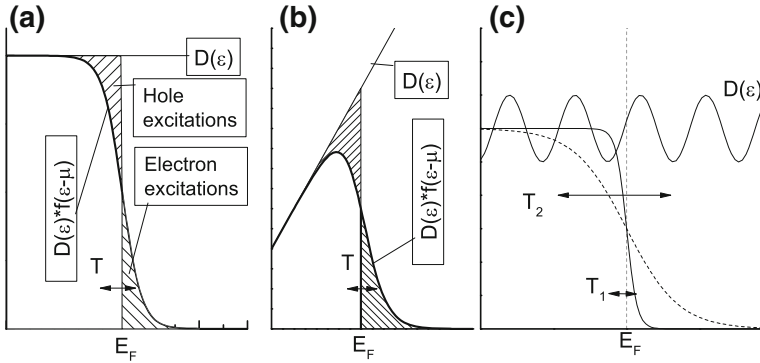


**Fig. 5** **a** Density of states  $D(\varepsilon) = \text{const}$  and its product with the Fermi distribution function. Equal hatched areas denote electron and hole excitations. **b** The same as (a) for the density of states changing with energy; the hatched areas are unequal. **c** Oscillatory density of states in perpendicular magnetic field and Fermi function corresponding to low temperature ( $T < \hbar\omega_c, \Gamma$ , solid line) and high temperature ( $T > \hbar\omega_c, \Gamma$ , dashed line)(Color figure online)

Hence, we find

$$\left(\frac{\partial\mu}{\partial T}\right)_n = -\frac{\pi^2 T}{3D(E_F)} \frac{\partial D(E_F)}{\partial E_F} = -\frac{\pi^2 T}{3} \frac{\partial D(E_F)}{\partial n}. \tag{3}$$

We note that this equation is applicable for degenerate Fermi systems of any dimensionality and for any spectrum.

In perpendicular field, due to Landau quantization,  $D(\varepsilon)$  becomes dependent on energy (see Fig. 5c), and Eq. (3) should be averaged over  $T$  in the vicinity of the Fermi energy. If the temperature is low ( $T_1$ , Fig. 5c), one can directly apply Eq. (3); in the opposite limit of high temperature ( $T_2$ , Fig. 5c) the oscillations are averaged over a wide energy interval and become exponentially suppressed.

Two qualitative predictions follow from the above considerations. (i) In the maxima and minima of the density of states the  $\partial\mu/\partial T$  signal is zero, and the signal is maximal at such field where the derivative  $\partial \ln D(E_F)/\partial E_F$  is maximal. (ii) The amplitude of the  $\partial\mu/\partial T$  magnetooscillations is a non-monotonic function of temperature: at low temperatures  $T \ll \omega_c, \Gamma$  the  $\partial\mu/\partial T$  increases with  $T$ , whereas for high temperatures,  $T \gtrsim \omega_c$ , averaging over several oscillations suppresses the signal.

The thermodynamic potential of non-interacting electron system can be written as [33]

$$\Omega(T, \mu, B) = -T \int d\varepsilon D(\varepsilon) \ln \left[ 1 + e^{(\mu-\varepsilon)/T} \right]. \tag{4}$$

In the presence of the perpendicular magnetic field  $B$  the density of states becomes

$$D(\varepsilon) = \frac{m\omega_c}{2\pi} \sum_{\sigma=\pm} \sum_{n=0}^{\infty} \mathcal{W}(\varepsilon + \sigma Z - \omega_c(n + 1/2)), \tag{5}$$

where  $Z = g_L \mu_B B/2$  ( $g_L$  stands for the  $g$ -factor) describes the effect of the Zeeman splitting. The function  $\mathcal{W}(\varepsilon)$  describes disorder broadening of a Landau level. It satisfies the normalization condition:  $\int d\varepsilon \mathcal{W}(\varepsilon) = 1$ . We note that, in general, this function can be different for different Landau levels. Using the function  $\mathcal{W}(\varepsilon)$  a typical width of a Landau level can be estimated as  $\Gamma \sim [\int d\varepsilon \mathcal{W}''(\varepsilon)]^{-1/2}$ . The accurate quantum-mechanical evaluation of  $\mathcal{W}(\varepsilon)$  for a given type of disorder is a complicated problem and solved only partially. In the absence of disorder one obviously has  $\mathcal{W}(\varepsilon) = \delta(\varepsilon)$ .

In a standard way by means of the Poisson resummation formula applied to the thermodynamic potential (4), we obtain the Lifshitz–Kosevich-type [34] expression for  $\partial\mu/\partial T$ :

$$\begin{aligned} \left(\frac{\partial\mu}{\partial T}\right)_T = & - \sum_{k=1}^{\infty} \frac{2\pi(-1)^k \mathcal{A}_k}{\sinh \mathcal{X}_k} \left[1 - \mathcal{X}_k \coth \mathcal{X}_k\right] \sin \frac{2\pi\mu k}{\omega_c} \\ & \times \cos \frac{2\pi Z k}{\omega_c} \left[1 + 2 \sum_{k=1}^{\infty} \frac{(-1)^k \mathcal{A}_k \mathcal{X}_k}{\sinh \mathcal{X}_k} \cos \frac{2\pi\mu k}{\omega_c} \right. \\ & \left. \times \cos \frac{2\pi Z k}{\omega_c} \right]^{-1}. \end{aligned} \quad (6)$$

This result holds for  $\mu \pm Z \gg \omega_c, T, \Gamma$ . Here  $\mathcal{X}_k = 2\pi^2 T k / \omega_c$ , and

$$\mathcal{A}_k = \int d\varepsilon \mathcal{W}(\varepsilon) \exp\left(\frac{2\pi i \varepsilon k}{\omega_c}\right) \quad (7)$$

characterizes damping of oscillations due to Landau level broadening.

For low temperatures,  $T \ll \omega_c, \Gamma, \mu \pm Z$ , the  $\partial\mu/\partial T$  value is given by Eq. (3) with  $D = (1/2) \sum_{\sigma=\pm} D(E_F^\sigma)$ . Here  $E_F^\sigma = 2\pi n_\sigma / m$  denotes the Fermi energy for a given spin projection. The corresponding electron density is determined by the Zeeman splitting,  $n_\sigma / n = 1 + \sigma Z / E_F$ , where  $E_F = 2\pi n / m$ . In the case of the Lorentzian broadening of a Landau level the density of states at the Fermi energy becomes [11]

$$D(E_F^\sigma) = \frac{m}{\pi} \frac{(1/2) \sinh(2\pi\Gamma/\omega_c)}{\sinh^2(\pi\Gamma/\omega_c) + \cos^2(\pi E_F^\sigma/\omega_c)}. \quad (8)$$

We mention that above we ignored the effect of electron-electron interaction. It is well known that for an interacting 3D electron system the Lifshitz–Kosevich-type expressions for magnetooscillations of the thermodynamic potential is modified via standard Fermi-liquid renormalization of the quasiparticle spectrum [35,36]. In 2D, in general it is not the case [37]. For classically weak perpendicular magnetic field modification of the Lifshitz–Kosevich-type expression for a 2D electron interacting disordered system has been studied in Refs. [38,39].

We studied two Schottky gated GaAs/AlGaAs single heterojunctions (GaAs1 and GaAs2, similar to those in Ref. [40]) with electron mobilities 20 and 25 m<sup>2</sup>/Vs,

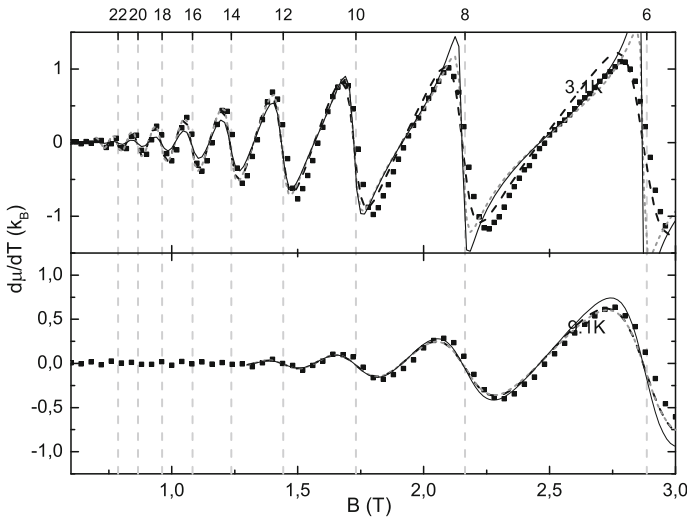


**Fig. 6**  $\partial\mu/\partial T$  versus magnetic field measured with sample GaAs2 at  $n = 4.16 \times 10^{11} \text{cm}^{-2}$ . Data are fitted with Lorentzian (*dashed curves*), Gaussian (*solid curves*), and Gaussian with  $\Gamma \propto \sqrt{B}$  (*dotted curves*) lineshapes at 3K (*panel a*) and 9K (*panel b*)

respectively, in the temperature range between 2.5 and 25K. The density could be varied in the range from  $2 \times 10^{11}$  to  $4 \times 10^{11} \text{cm}^{-2}$  by varying the gate voltage. The samples had  $5 \text{mm}^2$  area; the gate-to-2D gas capacitance was 1.1 nF. Both samples demonstrated similar results, we present therefore the data only for one sample, GaAs2.

Examples of the measured low-field  $\partial\mu/\partial T$  oscillations are shown in Fig. 6. For the fields lower than 3 Tesla and in the range of temperatures 2.7–9.1 K, we fitted the data using Eq. (6) with the bare band mass  $m_b = 0.067m_e$  [6]. Because of the low-field range used and large cyclotron splitting, all the results below are insensitive to the g-factor value (that may vary in the range  $g = -0.4/2$ ). The best fit is obtained for the broadening of Landau levels described by the Lorentzian model with the independent of  $B$  width  $\Gamma = 0.4 \text{meV}$  (see dashed curves in Fig. 6). The range of temperatures ( $0.22 \text{mV} < T < 0.8 \text{mV}$ ) and magnetic fields ( $0.86 < \hbar\omega_c < 5.2 \text{mV}$ ) used for fitting procedure is wide enough to identify the line shape with the Lorentzian curve. Other models for  $\Gamma$  fail to fit the oscillations (see Fig. 6). We checked that in a density range from  $3 \times 10^{11}$  to  $5 \times 10^{11} \text{cm}^{-2}$  the low-field level broadening is constant (equal to 0.4 meV for sample GaAs-2). The Lorentzian lineshape of the Landau levels is in the agreement with magnetization measurements of Potts et al. [41] on the moderate mobility GaAs-based sample; it is also in line with Gaussian lineshape with oscillatory level broadening [1,4].

It is appropriate to compare here the two techniques: the described above entropy measurements and the conventional technique of the specific heat measurements. The method described above allows us to measure  $\partial S/\partial n$ , whereas the ac calorimetry measures specific heat  $T\partial S/\partial T$ . Both methods, however, allow one to evaluate the entropy change. In the quantizing regime, when the entropy oscillates, one can integrate both  $\partial S/\partial n$  and  $T\partial S/\partial T$  and calculate the respective changes in entropy between the

neighboring maxima and minima. We compare the smallest oscillation one may detect with each particular method. The ac calorimetry measurements with a sample at density  $8.8 \times 10^{11} \text{ cm}^{-2}$ , mobility  $10 \text{ m}^2/\text{Vs}$  (both comparable to our GaAs1 sample), and in a similar temperature range (1.7–4.6 K) were done with a stack of 75 quantum wells, with 50 times larger total area [42]. The smallest oscillation was observed at filling factor = 12 in field of 3 Tesla. In our measurements with GaAs1 sample (Fig. 1 in [11]) at 2.5 K, we observed huge oscillations at the same field 3 Tesla. The oscillations were clearly observed down to 1 Tesla, where they had a factor of 50 lower amplitude. This implies that our technique has  $\sim 50 \times 50 = 2500$  times better sensitivity per unit area than the ac calorimetry. Remarkably, the  $(\partial S/\partial n)$  value we measure is of purely electronic origin and has no contribution from the lattice specific heat.

## 6 Conclusions

We presented here experimental test of the novel techniques of thermodynamic  $\partial\mu/\partial B$  and  $\partial\mu/\partial T$  measurements, which are ideally suitable for 2D gated carrier systems. The techniques are highly sensitive and thereby enable thermodynamic measurements with a single-layer electron system comprising only  $10^8$ – $10^{10}$  electrons. Particularly, the temperature modulation technique is three orders of magnitude superior in sensitivity to the ac calorimetry, allowing entropy measurements with only  $10^8$  electrons. The spin magnetization measurements provide evidence for an easily polarizable electron state in a wide density range from insulating to deep into the metallic phase.

The temperature and magnetic field dependence of the observed magnetization is consistent with the formation of large-spin droplets in the insulating phase. These droplets melt in the metallic phase with increasing density and temperature, though they survive up to large densities.

For the  $\partial\mu/\partial T$  magnetooscillations in 2D systems we also present a Lifshits–Kosevitch-type calculations and compare the theory with experimental data; the comparison reveals a good agreement between the data and the theory. The magnetic field dependence of the  $\partial\mu/\partial T$  appears to be rather sensitive to the shape of the density of states at Landau levels.

Both magnetic field and temperature modulation techniques enable measurements down to very low electron densities which are inaccessible for transport measurements.

**Acknowledgments** AYuK acknowledges support by RFBR (15-02-07715); VMP and ISB acknowledge support by RSF (14-12-00879). MR was supported by ISF, Grant No. 1445/11. Measurements at LPI were performed using research equipment of the LPI shared facility center.

## References

1. V.M. Pudalov, S.G. Semenchinskii, V.S. Edel'man, ZhETF **89**, 1870 (1985). [JETP **62**, 1079 (1985)]
2. V.M. Pudalov, S.G. Semenchinskii, V.S. Edel'man, Pis'ma v ZhETF **41**, 225 (1985). [JETP Lett. **41**, 325 (1985)]
3. R.T. Zeller, B.B. Goldberg, P.J. Stiles, F.F. Fang, S.L. Wright, Phys. Rev. B **33**, 1529R (1986)
4. V.M. Pudalov, S.G. Semenchinskii, Pis'ma ZhETF **44**(11), 526 (1986). [JETP Lett. **44**(11), 677 (1986)]
5. W. Thomson, Phil. Mag. **46**, 82 (1898)
6. T. Ando, A.B. Fowler, F. Stern, Rev. Mod. Phys. **54**(2), 437 (1982)

7. J.P. Eisenstein, L.N. Pfeiffer, K.W. West, Phys. Rev. B. **50**, 1760 (1994)
8. S.V. Kravchenko, V.M. Pudalov, D.A. Rinberg, S.G. Semenchinsky, Phys. Lett. A **146**, 535 (1990)
9. N. Teneh, AYu. Kuntsevich, V.M. Pudalov, M. Reznikov, Phys. Rev. Lett. **109**, 226403 (2012)
10. V.I. Nizhankovskii, Europ. Phys. J. B **3**(18), 397 (2000)
11. Y. Tupikov, AYu. Kuntsevich, V.M. Pudalov, I.S. Burmistrov, Pisma v ZhETF **101**, 131 (2015). [JETP Lett. **101**, 125 (2015)]
12. A.Yu. Kuntsevich, Y.V. Tupikov, V.M. Pudalov, and I.S. Burmistrov, /ncomms8298
13. G. Giuliani, G. Vignale, *Quantum Theory of the Electron Liquid* (Cambridge University Press, Cambridge, 2005)
14. B. Tanatar, D.M. Ceperley, Phys. Rev. B **39**, 5005 (1989)
15. A.C. Eguluz, A.A. Maradudin, R.J. Elliott, Phys. Rev. B **27**, 4933 (1983)
16. S.T. Chui, B. Tanatar, Phys. Rev. Lett. **74**, 458 (1995)
17. S.T. Chui, B. Tanatar, Phys. Rev. B **55**, 9330 (1997)
18. V.M. Pudalov, M. D'Iorio, S.V. Kravchenko, J.W. Campbell, Phys. Rev. Lett. **70**, 1866 (1993)
19. M.S. Bello, E.I. Levin, B.I. Shklovskii, A.L. Efros, Zh. Eksp. Teor. Fiz. **80**, 1596 (1981). [Sov. Phys. JETP **53**, 822 (1981)]
20. A.L. Efros, Solid State Commun. **65**, 1281 (1988)
21. S.V. Kravchenko, V.M. Pudalov, S.G. Semenchinsky, Phys. Lett. A **141**, 71 (1989)
22. S.V. Kravchenko, D.A. Rinberg, S.G. Semenchinsky, V.M. Pudalov, Phys. Rev. B **42**(6), 3741 (1990)
23. J.P. Eisenstein, L.N. Pfeiffer, K.W. West, Phys. Rev. Lett. **68**, 674 (1992)
24. J.P. Eisenstein, L.N. Pfeiffer, K.W. West, Phys. Rev. B **50**, 1760 (1994)
25. S. Shapira et al., Phys. Rev. Lett. **77**, 3181 (1996)
26. S.C. Dultz, H.W. Jiang, Phys. Rev. Lett. **84**, 4689 (2000)
27. A.H. MacDonald, H.C.A. Oji, K.L. Liu, Phys. Rev. B **34**, 2681 (1986)
28. Y. Zhang, S. Das Sarma, Phys. Rev. B **72**, 115317 (2005)
29. C. Attacalite, S. Moroni, P. Gori-Giorgi, G.B. Bachelet, Phys. Rev. Lett. **88**, 256601 (2002)
30. O. Prus, Y. Yaish, M. Reznikov, U. Sivan, V. Pudalov, Phys. Rev. B **67**, 205407 (2003)
31. A.A. Shashkin, S. Anissimova, M.R. Sakr, S.V. Kravchenko, V.T. Dolgoplov, T.M. Klapwijk, Phys. Rev. Lett. **96**, 036403 (2006)
32. M. Reznikov, AYu. Kuntsevich, N. Teneh, V.M. Pudalov, Pis'ma v ZhETF **92**, 518–522 (2010)
33. L.D. Landau, E.M. Lifshitz, *Statistical Physics. Part I, Course of Theoretical Physics*, vol. 5 (Butterworth-Heinemann, Oxford, 1980)
34. I.M. Lifshitz, A.M. Kosevich, JETP **2**, 636 (1956)
35. J.M. Luttinger, Phys. Rev. **121**, 1251 (1961)
36. YuA Bychkov, L.P. Gor'kov, JETP **14**, 1132 (1962)
37. S. Curnoe, P.C.E. Stamp, Phys. Rev. Lett. **80**, 3312 (1998)
38. G.W. Martin, D.L. Maslov, MYu. Reizer, Phys. Rev. B **68**, 241309(R) (2003)
39. Y. Adamov, I.V. Gornyi, A.D. Mirlin, Phys. Rev. B **73**, 045426 (2006)
40. V.G. Mokerov, B.K. Medvedev, V.M. Pudalov, D.A. Rinber, S.G. Semenchinsky, YuV Slepnev, JETP Lett. **47**, 59 (1988)
41. A. Potts, R. Shepherd, W.G. Herrenden-Harker, M. Elliott, C.L. Jones, A. Usher, G.A.C. Jones, D.A. Ritchie, E.H. Linfield, M. Grimshaw, J. Phys. **8**, 5189 (1996)
42. J.K. Wang, J.H. Campbell, D.C. Tsui, A.Y. Cho, Phys. Rev. B **38**, 6174 (1988)